nature photonics

CORRECTED ONLINE: 15 APRIL 2009
PUBLISHED ONLINE: 11 JANUARY 2009 | DOI: 10.1038/NPHOTON.2008.273

LETTERS

Complete optical isolation created by indirect interband photonic transitions

Zongfu Yu[1] and Shanhui Fan[2]*

Achieving on-chip optical signal isolation is a fundamental difficulty in integrated photonics[1]. The need to overcome this difficulty is becoming increasingly urgent, especially with the emergence of silicon nano-photonics[2-4], which promises to create on-chip optical systems at an unprecedented scale of integration. Until now, there have been no techniques that provide complete on-chip signal isolation using materials or processes that are fundamentally compatible with silicon CMOS processes. Based on the effects of photonic transitions[5,6], we show here that a linear, broadband and non-reciprocal isolation can be accomplished by spatial–temporal refractive index modulations that simultaneously impart frequency and wavevector shifts during the photonic transition process. We further show that a non-reciprocal effect can be accomplished in dynamically modulated micrometre-scale ring-resonator structures. This work demonstrates that on-chip isolation can be accomplished with dynamic photonic structures in standard material systems that are widely used for integrated optoelectronic applications.

Creating complete optical signal isolation requires time-reversal symmetry breaking. In bulk optics, this is achieved using materials exhibiting magneto-optical effects. Despite many attempts[7–10], on-chip integration of magneto-optical materials is still difficult to achieve, particularly in silicon, in a CMOS-compatible fashion. Optical isolation has also been observed using nonlinear optical processes[11,12] and in electro-absorption modulators[13]. In these cases, however, optical isolation occurs only for specific power ranges[11,12] or with associated modulation side bands[13]. In addition, there have been works that aim to achieve partial optical isolation in reciprocal structures that have no inversion symmetry (for example, chiral structures). In these systems, the apparent isolation occurs only if the allowed photon states in the backward direction is restricted and would not work for arbitrary backward incoming states. None of the non-magnetic schemes achieved to date can provide complete optical isolation.

In this Letter, we show that complete optical isolation can be achieved dynamically by inducing indirect photonic transitions in an appropriately designed photonic structure. It has been shown theoretically[5] that when photonic structures are subject to temporal refractive-index modulation, photon states can go through interband transitions, in a direct analogy to electronic transitions in semiconductors. Such photonic transitions have recently been demonstrated experimentally in silicon micro-ring resonators[6]. (We note that such a transition is different from the adiabatic wavelength conversion process[14–18] in that the transition involves at least two photonic states.) Building on these advancements, we show that by appropriately designing a band structure, and by choosing a spatially and temporally varying modulation format that simultaneously imparts frequency and momentum shifts of photon states during the transition process (Fig. 1a), the transmission behaviour of a photonic structure can become non-reciprocal—light of

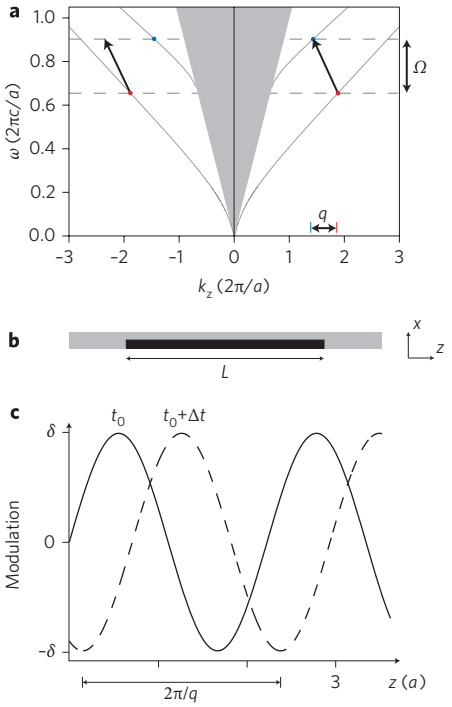

Figure 1 | Schematic of indirect photonic transition in a silicon slab waveguide. a, Band structure of a silicon waveguide. The width of the waveguide is 0.22 μm. The angular frequency and wavevectors are normalized with respect to $a = 1$ μm. Red (blue) dots indicate modes at frequency ω_1 (ω_2) in the first (second) band. The arrows indicate frequency and wavevector shifts as induced by a dynamic modulation shown in **b** and **c. b**, Structure of the silicon waveguide ($\varepsilon_s = 12.25$). Modulation is applied to the dark region. **c**, The modulation profile at two sequential time steps.

frequency ω_1 in the forward direction is converted to a higher frequency mode ω_2 by the modulation. At the same time, such a modulation has no effect on the light propagating in the backward direction at all frequencies and therefore leaves the mode in the backward direction intact. Combined with an absorption filter centred at ω_2, this structure can absorb all light incident from one direction at ω_1, while passing those in the opposite direction, and thus create the behaviour of a complete isolator.

We start by demonstrating such dynamic processes in a silicon waveguide. The waveguide (assumed to be two-dimensional) is represented by a dielectric distribution $\varepsilon_s(x)$ that is time-independent and uniform along the z-direction. Such a waveguide possesses a band structure as shown in Fig. 1a, with symmetric and antisymmetric modes located in the first and second bands, respectively. An interband

[1]Department of Applied Physics, Stanford University, Stanford, California 94305, USA, [2]Department of Electrical Engineering, Stanford University, Stanford, California 94305, USA; *e-mail: shanhui@stanford.edu

transition, between two modes with frequencies and wavevectors (ω_1, k_1), (ω_2, k_2) located in these two bands, can be induced by modulating the waveguide with an additional dielectric perturbation

$$\varepsilon'(x,z,t) = \delta(x)\cos(\Omega t - (-q)z) \quad (1)$$

where $\delta(x)$ is the modulation amplitude distribution along the direction transverse to the waveguide. Here, the modulation frequency $\Omega = \omega_2 - \omega_1$. Such a transition, with $k_1 \neq k_2$, is referred to in this paper as an 'indirect photonic transition', in analogy with indirect electronic transitions in semiconductors. We assume the wavevector shift q approximately satisfies the phase-matching condition, that is, $\Delta k = k_2 - k_1 - (-q) \approx 0$. In the modulated waveguide, the electric field becomes

$$E(x,z,t) = a_1(z)E_1(x)e^{i(-k_1 z+\omega_1 t)} + a_2(z)E_2(x)e^{i(-k_2 z+\omega_2 t)} \quad (2)$$

where $E_{1,2}(x)$ are the modal profiles, normalized such that $|a_n|^2$ is the photon number flux carried by the nth mode. By substituting equation (2) into Maxwell's equations, and using a slowly varying envelope approximation, we can derive the coupled-mode equation

$$\frac{\mathrm{d}}{\mathrm{d}z}\begin{pmatrix} a_1 \\ a_2 \end{pmatrix} = \begin{pmatrix} 0 & iC\exp(-i\Delta k z) \\ iC\exp(i\Delta k z) & 0 \end{pmatrix}\begin{pmatrix} a_1 \\ a_2 \end{pmatrix} \quad (3)$$

where $C = \frac{\varepsilon_0}{8}\int_{-\infty}^{\infty}\delta(x)E_1(x)E_2(x)\mathrm{d}x$ is the coupling strength. With an initial condition $a_1(0) = 1$ and $a_2(0) = 0$, the solution to equation (3) is

$$a_1(z) = e^{-iz\Delta k/2}\left[\cos\left(z\sqrt{C^2 + (\Delta k/2)^2}\right) + i\frac{\Delta k/2}{\sqrt{C^2 + (\Delta k/2)^2}}\sin\left(z\sqrt{C^2 + (\Delta k/2)^2}\right)\right]$$

$$a_2(z) = ie^{iz\Delta k/2}\frac{C\sin\left(z\sqrt{C^2 + (\Delta k/2)^2}\right)}{\sqrt{C^2 + (\Delta k/2)^2}} \quad (4)$$

In the case of perfect phase-matching, that is, $\Delta k = 0$, a photon initially in mode 1 will make a complete transition to mode 2 after propagating over a distance of coherence length $l_c = \pi/2|C|$. In contrast, in the case of strong phase-mismatch, that is, $|\Delta k| \gg 0$, the transition amplitude is negligible.

The system as shown in Fig. 1a exhibits strong non-reciprocal behaviour—the modulation in equation (1) does not phase-match the mode at (ω_1, $-k_1$) with any other mode of the system. Thus, while the mode at (ω_1, k_1) undergoes a complete photonic transition, its time-reversed counterpart at (ω_1, $-k_1$) is not affected at all. Such non-reciprocity arises from the breaking of both time-reversal and spatial-inversion symmetries in the dynamics—the modulation in equation (1) is not invariant with either $t \rightarrow -t$ or $z \rightarrow -z$.

To verify the above theory, we numerically simulated the dynamic process by solving Maxwell's equations using a finite-difference time-domain (FDTD) method[19]. The width of the waveguide was chosen to be 0.22 μm, such that the waveguide supports a single transverse electric mode at the 1.55 μm wavelength range. To maximize the coupling strength, the modulation region was chosen to occupy half the waveguide width (Fig. 1b). Figure 1c shows the profile of such dynamic modulation at two sequential time steps, with a phase-matching condition that induces a transition between mode 1 at $\omega_1 = 0.6468(2\pi c/a)$ and mode 2 at $\omega_2 = 0.8879(2\pi c/a)$. For visualization purposes, we chose a large modulation strength ($\delta_{\max}/\varepsilon = 1/12.25$, where $\delta_{\max}$ is the maximum value of modulation strength and ε the dielectric constant of silicon) such that the effect could be observed with a relatively short waveguide.

In the simulation, we first chose the length of the modulation region ($=20a$) to be much longer than the coherence length. A continuous wave at ω_1 was launched at the left end of the structure. As the wave propagated along the $+z$ direction, part of the amplitude was converted to ω_2. The intensities of the waves at the two frequencies oscillated sinusoidally along the propagation direction (Fig. 2a), while conserving the total numbers of photons. From the simulation, the coherence length l_c was determined to be $10.2a$.

To demonstrate non-reciprocal frequency conversion, the length of the modulation region was chosen to be the coherence length, $L = l_c$ (Fig. 1b). We chose an incident light pulse with a Gaussian spectrum centred at ω_1 (Fig. 2b). A pulse incident from the left was completely converted to a pulse centred at ω_2 (Fig. 2c). The mode profile thus completely converted from symmetric to anti-symmetric after passing through the modulated region (Fig. 2c, inset). In contrast, the same pulse, when incident from the right, passed through the structure unperturbed (Fig. 2d). This structure therefore provides complete contrast between forward and backward directions. In addition, we have also observed that incident light from the right at around ω_2 does not experience any frequency conversion. The response of the system is certainly not time-reversal invariant.

In Fig. 2a we also show excellent agreement between the theory of equation (3) and numerical simulation. In the theory, there is no free parameter. All parameters in equation (3) are determined analytically. We note that the coupled-mode theory becomes exact in the limit of small index modulation (that is, $\delta \rightarrow 0$). Because the index modulation achievable in experiments is typically far smaller than that we use here in the simulations, the excellent agreement between theory and simulation indicates that the coupled-mode theory can be directly applied in experimental situations.

Using the theory of equation (3), we now perform designs assuming an index modulation strength of $\delta/\varepsilon = 5 \times 10^{-4}$, and a modulation frequency of 20 GHz, both of which are achievable in state-of-the-art silicon modulators[6,20]. Such a modulation induces a transition from a first band mode at 1.55 μm to a second band mode 20 GHz higher in frequency. With a choice of the width of the waveguide of 0.27 μm, complete non-reciprocal conversion occurs with a coherence length $l_c = 2.19$ mm.

This waveguide width of 0.27 μm was chosen to create transitions between two parallel bands with matching group velocity. Such a parallel band configuration is optimal because it ensures broadband operation—a modulation that phase-matches between (ω_1, k_1) and ($\omega_2 = \omega_1 + \Omega$, $k_2 = k_1 + (-q)$) automatically phase-matches for all incident frequencies in the vicinity of ω_1. For this device, our calculation indicates that over a frequency bandwidth of 1.2 THz, the contrast ratio between forward and backward transmission coefficients is above 20 dB. (See Supplementary Information for details of this calculation.)

We would like to emphasize that the modulation frequency can be far smaller than the bandwidth of the signal. This is in fact one of the key advantages of making use of the interband transition. The transition occurs from a fundamental even mode to a second-order odd mode. The generated odd mode can be removed with the use of mode filters that operate on the basis of modal profiles. Examples of such mode filters can be found in refs 21 and 22. It is important to point out that such mode filters are purely passive and reciprocal, and can be readily implemented on-chip in a very compact fashion.

The required modulation profile here has a low frequency in the radio-frequency range, and a large wavevector corresponding to a spatial period in the micrometre range. Such a modulation profile

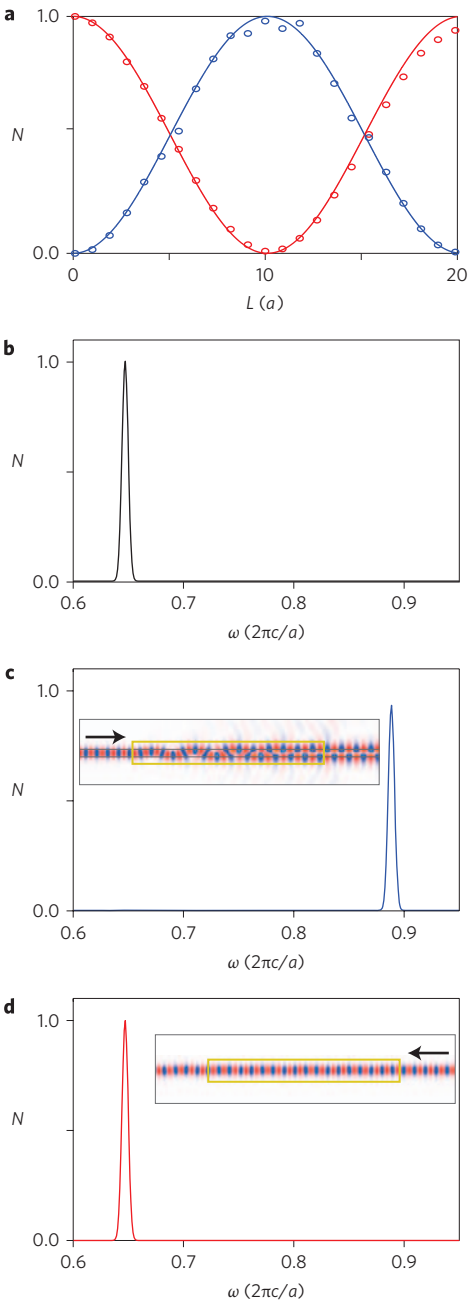

Figure 2 | Non-reciprocal frequency conversion in a waveguide. **a**, Spatial evolution of the photon flux N of two modes, when a phase-matching modulation is applied to the waveguide. Red (mode 1) and blue (mode 2) solid lines represent analytical theory and circles are from FDTD simulation. **b**, The spectrum of photon flux in the incident pulse. **c**,**d**, Transmitted photon flux spectra when the direction of incidence of the pulse in **b** is from the left (**c**) or the right (**d**). The insets show the distribution of electric fields from FDTD simulation, with continuous-wave excitation at ω_1. The arrows represent the direction of incidence and the yellow rectangle indicates the modulated waveguide region.

is quite different from what is typically used in travelling-wave electro-optic modulators and represents a new operating regime. Instead, such modulation can in principal be achieved by standing-wave modulation of a set of discrete regions, each modulated at a different phase. These discrete regions can be made so that they are electrically separated, for example, by etching grooves between them, as it is well known that a waveguide with a periodic array of

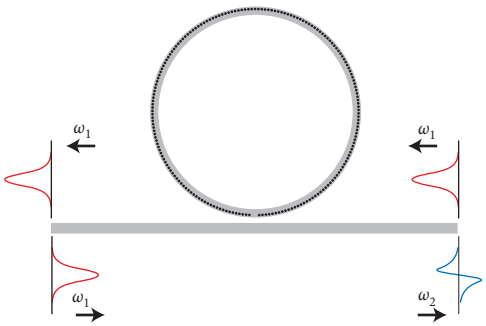

Figure 3 | Schematic of a ring resonator designed for non-reciprocal frequency conversion. The dark regions are modulated. The diameter of the rods is 0.08a with their centres along a circle of radius $R = 3.08a$. The spacing between centres of two adjacent circles is 0.1a.

air grooves supports guided modes that are intrinsically lossless when the periodicity is at submicrometre scales[23].

In general, non-reciprocal effects can also be observed in intra-band transitions. However, because, typically, $\Omega \ll \omega_1$, and the dispersion relation of a single band can typically be approximated as linear in the vicinity of ω_1, a cascaded process[6] that generates frequencies at $\omega_1 + n\Omega$ (with $n > 1$) is unavoidable, complicating the device performance. Our use of the interband transition, however, eliminates such cascaded processes.

Further reduction of the device footprint can be accomplished using a resonator structure. As an example, we formed a ring resonator (Fig. 3) with the same waveguide as in Fig. 1b with a width of 0.22 μm. The centre of the ring waveguide was a circle with a radius of 3 μm, chosen such that two modes at $\omega_1 = 0.6468(2\pi c/a)$ and $\omega_2 = 0.8879(2\pi c/a)$ were both resonant. The ring was coupled to an external waveguide with a width 0.23 μm. The edge-to-edge distance between the ring and the external waveguides was 0.18 μm, leading to external quality factors $Q_{c1} = 3{,}426$ and $Q_{c2} = 887$ for the two modes due to waveguide–cavity coupling. The two modes also had radiation quality factors of $Q_{r1} = 1.9 \times 10^4$ and $Q_{r2} = 2.3 \times 10^4$. The modulation area consisted of an array of discrete regions along the ring (Fig. 3). We chose a modulation strength $\delta/\varepsilon = 4.75 \times 10^{-3}$, resulting in a coherence length of $l_c = 250$ μm. The ring circumference was therefore far smaller than the coherence length.

Figure 4a,b shows a simulation of the structure with a steady-state input. Incident light at ω_1 from the left (Fig. 4a) is converted to ω_2. Note that the mode profile in the external waveguide changes from symmetric to antisymmetric after light passes through the ring. In contrast, no conversion is observed for light input from the right. The field profile remains symmetric in the external waveguide after the light passes through the ring (Fig. 4b).

Figure 4c,d shows the output spectra when the input has a Gaussian spectrum centred at ω_1. For light coming from the left, the simultaneous presence of a dip in the vicinity of ω_1 and a peak in the vicinity of ω_2 indicates a strong frequency conversion effect (Fig. 4c). The maximum conversion efficiency is about 80%; the rest is lost due to the intrinsic radiation loss of the cavity. In contrast, for light incident from the opposite direction (Fig. 4d), the output spectrum shows no feature at ω_2, indicating the absence of frequency conversion. The dip at ω_1 is due purely to the intrinsic radiation loss of the ring. The numerical simulation shows excellent agreement with theoretical calculation (as detailed in the Supplementary Information). In comparison to the waveguide case, the results here demonstrate an ultra-compact non-reciprocal device, obtained at the expense of a reduced operational bandwidth. The ring resonant device can also operate with low modulation frequency in the 20 GHz range. For efficient transition both

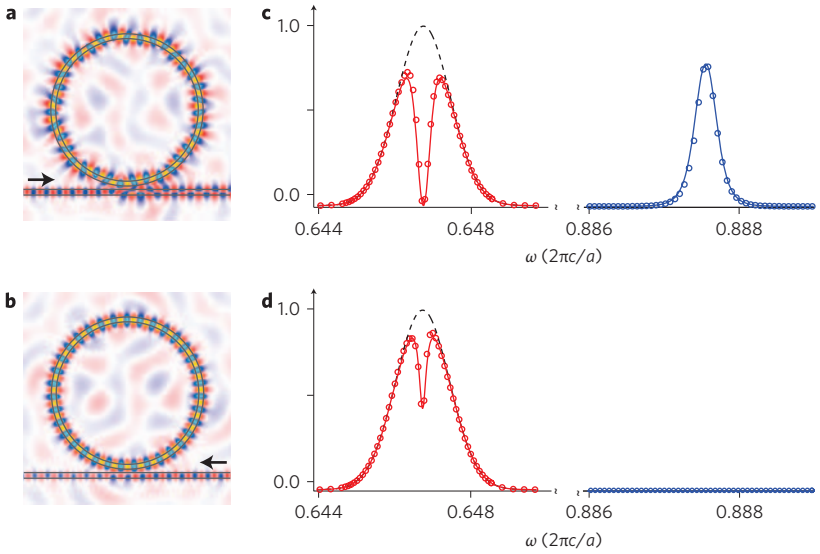

Figure 4 | Field distribution and frequency response of the modulated coupled ring–waveguide structure. Lights are incident from the left (**a**,**c**) and the right (**b**,**d**). **a**,**b** Distribution of electric fields with continuous wave incident at ω_1. **c**,**d** The output spectra. The dashed lines are the input spectra. The solid lines are the output spectra calculated analytically. The circles represent data from the FDTD simulation.

states involved need to be on-resonance in the ring. With the same modulation profile for the waveguide case (as discussed in the Supplementary Information), one can ensure that such a double resonance condition is satisfied along only one rotation direction inside the ring.

Finally, in contrast to previously considered isolators based on material nonlinearity[11,12], where isolation is only achievable for high incident power, the photonic transition effect studied here is linear with respect to the incident light; the effect does not depend upon the amplitude and phase of the incident light. Having a linear process is crucial because the device operation needs to be independent of the format, the timing and the intensity of the pulses used in the system. In conclusion, the structure proposed here shows that on-chip isolation can be accomplished with dynamic modulation in standard material systems that are widely used for integrated opto-electronic applications.

Received 4 June 2008; accepted 1 December 2008; published online 11 January 2009

References

1. Soljacic, M. & Joannopoulos, J. D. Enhancement of nonlinear effects using photonic crystals. *Nature Mater.* **3,** 211–219 (2004).
2. Pavesi, L. & Lockwood, D. J. *Silicon Photonics* (Springer, 2004).
3. Almeida, V. R., Barrios, C. A., Panepucci, R. R. & Lipson, M. All-optical control of light on a silicon chip. *Nature* **431,** 1081–1084 (2004).
4. Miller, D. A. B. Optical interconnects to silicon. *IEEE J. Sel. Top. Quant. Electron.* **6,** 1312–1317 (2000).
5. Winn, J. N., Fan, S., Joannopoulos, J. D. & Ippen, E. P. Interband transitions in photonic crystals. *Phys. Rev. B* **59,** 1551–1554 (1998).
6. Dong, P., Preble, S. F., Robinson, J. T., Manipatruni, S. & Lipson, M. Inducing photonic transitions between discrete modes in a silicon optical microcavity. *Phys. Rev. Lett.* **100,** 033904 (2008).
7. Espinola, R. L., Izuhara, T., Tsai, M. C., Osgood, R. M. Jr & Dötsch, H. Magneto-optical nonreciprocal phase shift in garnet/silicon-on-insulator waveguides. *Opt. Lett.* **29,** 941–943 (2004).
8. Levy, M. A nanomagnetic route to bias-magnet-free, on-chip Faraday rotators. *J. Opt. Soc. Am. B* **22,** 254–260 (2005).
9. Zaman, T. R., Guo, X. & Ram, R. J. Faraday rotation in an InP waveguide. *Appl. Phys. Lett.* **90,** 023514 (2007).
10. Dötsch, H. *et al.* Applications of magneto-optical waveguides in integrated optics: review. *J. Opt. Soc. Am. B* **22,** 240–253 (2005).
11. Soljaic, M., Luo, C., Joannopoulos, J. D. & Fan, S. Nonlinear photonic microdevices for optical integration. *Opt. Lett.* **28,** 637–639 (2003).
12. Gallo, K., Assanto, G., Parameswaran, K. R. & Fejer, M. M. All-optical diode in a periodically poled lithium niobate waveguide. *Appl. Phys. Lett.* **79,** 314–316 (2001).
13. Ibrahim, S. K., Bhandare, S., Sandel, D., Zhang, H. & Noe, R. Non-magnetic 30 dB integrated optical isolator in III/V material. *Electron. Lett.* **40,** 1293–1294 (2004).
14. Yariv, A. Electro-optic frequency modulation in optical resonators. *Proc. IEEE* **52,** 719–720 (1964).
15. Siegman, A. *Lasers* 986 (University Science Books, 1986).
16. Reed, E. J., Soljacic, M. & Joannopoulos, J. D. Reversed Doppler effect in photonic crystals. *Phys. Rev. Lett.* **91,** 133901 (2003).
17. Yanik, M. F. & Fan, S. Stopping light all-optically. *Phys. Rev. Lett.* **92,** 083901 (2004).
18. Notomi, M. & Mitsugi, S. Wavelength conversion via dynamic refractive index tuning of a cavity. *Phys. Rev. A* **73,** 051803(R) (2006).
19. Taflove, A. & Hagness, S. C. *Computational Electrodynamics: The Finite-Difference Time-Domain Method* 2nd edn (Artech House, 2000).
20. Preble, S. F., Xu, Q. & Lipson, M. Changing the colour of light in a silicon resonator. *Nature Photon.* **1,** 293–296 (2007).
21. Jiao, Y., Fan, S. & Miller, D. A. B. Demonstrations of systematic photonic crystal design and optimization by low rank adjustment: an extremely compact mode separator. *Opt. Lett.* **30,** 141–143 (2005).
22. Lee, B. T. & Shin, S. Y. Mode-order converter in a multimode waveguide. *Opt. Lett.* **28,** 1660–1662 (2003).
23. Fan, S. *et al.* Guided and defect modes in periodic dielectric waveguides. *J. Opt. Soc. Am. B* **12,** 1267–1272 (1995).

Acknowledgements

This work was supported in part by the National Science Foundation (grant no. ECS-0622212). S.F. acknowledges discussions with Z. Wang and M. Soljacic. The computations were performed at the Pittsburgh Supercomputing Center and the National Center for Supercomputing Applications, through the support of the National Science Foundation TeraGrid programme.

Additional information

Supplementary Information accompanies this paper at www.nature.com/naturephotonics. Reprints and permission information is available online at http://npg.nature.com/reprintsandpermissions/. Correspondence and requests for materials should be addressed to S.F.

CORRIGENDUM

Complete optical isolation created by indirect interband photonic transitions

Zongfu Yu and Shanhui Fan

Nature Photonics **3,** 91–94 (2009); published online: 11 January 2009; corrected online 15 April 2009.

The authors wish to correct equation (4) of the above Letter; it should have appeared as shown below. This also affects the final sentence in the third paragraph from the end of page 92, which should now read "For this device, our calculation indicates that over a frequency bandwidth of 1.2 THz, the contrast ratio between forward and backward transmission coefficients is above 40 dB." These errors have been corrected in the HTML and PDF versions of the Letter.

$$a_1(z) = e^{-iz\Delta k/2}\left[\cos\left(z\sqrt{C^2+(\Delta k/2)^2}\right) + i\frac{\Delta k/2}{\sqrt{C^2+(\Delta k/2)^2}}\sin\left(z\sqrt{C^2+(\Delta k/2)^2}\right)\right]$$

$$a_2(z) = ie^{iz\Delta k/2}\frac{C\sin\left(z\sqrt{C^2+(\Delta k/2)^2}\right)}{\sqrt{C^2+(\Delta k/2)^2}} \qquad (4)$$